Titanium Oxide Species in Molecular Sieves: Materials for the Optical Sensing of Reductive Gas Atmospheres

Gerd Grubert,[†,‡] Michael Stockenhuber,[§] Olga P. Tkachenko,[∥] and Michael Wark*[,‡]

Institute of Applied and Physical Chemistry, University of Bremen, D-28334 Bremen, Germany, Catalysis Research Laboratory, Nottingham Trent University, Clifton Campus, NG11 8NS, United Kingdom, and N.D. Zelinsky Institute of Organic Chemistry, Russian Academy of Sciences, Leninsky prospect 47, Moscow V-334, Russia

Received August 22, 2001. Revised Manuscript Received April 19, 2002

The reversible redox behavior of intrazeolitic titanium dioxide clusters in reducing and oxidizing atmospheres (H_2, CO, O_2) is studied by in situ diffuse reflectance UV/vis spectroscopy (UV/vis DRS). Titanium oxide species, mononuclearly dispersed or as clusters with a particle size up to 2 nm, have been stabilized in the pores of molecular sieves by chemical vapor deposition (cvd) or ion exchange from aqueous solutions and subsequent calcination. The structure of different Ti^{IV} oxide species and their location with respect to the zeolite matrix, that is, inside the pore system or on the external surface, has been deduced from (i) the blue shifts of absorption edges in diffuse reflectance UV/vis spectra, (ii) the interpretation of XANES and EXAFS spectra giving coordination numbers and bond lengths, (iii) XPS measurements, and (iv) the reduction behavior to Ti^{III}. The zeolite matrix ensures good stability of the highly dispersed Ti^{IV} oxide species. The response time of hosted Ti^{IV} oxide species for the optical registration of the presence of H_2 in surrounding gas atmospheres decreases with their decreasing cluster size and is lowest for mononuclear species with a highly distorted oxygen coordination sphere. In comparison to bulk TiO_2 the response times of Ti^{IV} oxide/zeolite composites is shortened by a factor of about 10 and are comparable to those values found for solid-state electrolyte sensors. Also, changes in the ratio of CO:air mixtures can easily be monitored.

1. Introduction

Oxygen sensing techniques are applied to various fields, such as chemical and clinical analysis and environmental monitoring.[1−3] The sensing systems are classified into a variety of categories, that is, titration,[4] chemiluminescence,[5] thermoluminescence,[6] and, the most popular, amperometry.[7] The most widely distributed commercial oxygen sensors are based on ZrO_2 (e.g., λ probe in vehicles) or SnO_2 (e.g., Taguchi sensor).[8,9] Also, the sensing properties of the bulk material or thin films of TiO_2 have been studied intensively.[10,11]

To achieve further miniaturization of sensing systems, research has been focused on the development of (metal oxide)-based materials in which their surface-to-volume ratio is drastically increased. Several attempts have been reported to develop TiO_2 phases of high porosity (>600 m^2/g) by template-assisted self-organization[12,13] or electrodeposition,[14] but highest dispersion can be achieved by stabilization of nanometer-sized TiO_2 particles.[15] Molecular sieves, for example, zeolites of the faujasite-type NaY, with their defined pore structures are suitable hosts for the storage of defined dispersions of very small mono- and polynuclear oxide clusters.[16,17] The zeolite matrix ensures good

* To whom correspondence should be addressed. Present address: Institute of Physical Chemistry, University of Hanover, Callin Str. 3-3A, D-30167 Hanover, Germany. E-mail: Michael.Wark@pci.uni-hannover.de. Fax: +49 511 19121.

† Present address: Institute for Applied Chemistry Berlin Adlershof e.V., Rudower Chaussee 12, D-12489 Berlin, Germany.

‡ University of Bremen.

§ Nottingham Trent University. Phone and Fax: +44 1159 48 6694. E-mail: Michael.Stockenhuber@ntu.ac.uk.

∥ Russian Academy of Sciences.

(1) Prininger, C.; Klimant, I.; Wolfbeis, O. S. *Anal. Chem.* **1994**, *66*, 1841.

(2) Martin, E. C.; Malin, S. F.; Bartnil, D. J.; Schilling, A. M.; Furlong, S. C. *Proc. SPIE* **1994**, *2131*, 426.

(3) Atkinson, M. J.; Thomas, F. I. M.; Larson, N.; Terrill, E.; Morita K.; Lium, C. C. *Deep-Sea Res.* I **1995**, *42*, 761.

(4) Skoog, D. A.; West, D. M.; Holler, F. J. *Fundamentals of Analytical Chemistry*; Saunders: Philadelphia, PA, 1988; p 344.

(5) Freeman, T. M.; Seitz, W. R. *Anal. Chem.* **1981**, *53*, 98.

(6) Hendricks, H. D. U.S. Patent 3,709,663, 1973.

(7) Clark, L. C. *Trans. Am. Artif. Intern. Organs.* **1956**, *2*, 41.

(8) Schaumburg, H. *Sensoren*; Teubner B. G. Press: Stuttgart, 1992; pp 437 ff.

(9) Takeuchi, T. *Sensors Actuators* **1988**, *14*, 109.

(10) Göpel, W.; Hesse, J.; Zemel, J. N. *Sensors*; VCH: Weinheim, 1989; Vol. 8, pp 182 ff.

(11) Tang, H.; Prasad, K.; Levy, F. *Sensors Actuators B* **1995**, *26/27*, 71.

(12) Antonelli, D. M.; Ying, J. Y. *Angew. Chem., Int. Ed. Engl.* **1996**, *35*, 426.

(13) Zhong, Z.; Yin, Y.; Gates, B.; Xia, Y. *Adv. Mater.* **2000**, *12*, 206.

(14) Matsumoto, Y.; Ishikawa, Y.; Nishida, M.; Ii, S. *J. Phys. Chem. B* **2000**, *104*, 4202.

(15) Serpone, N.; Lawless, D.; Khairutdinov, R. *J. Phys. Chem.* **1995**, *99*, 16646.

(16) (a) Wark, M.; Grubert, G. In *Proceedings of the EUROMAT 99 conference, Volume 9 "Interface Controlled Materials"*; Rühle, M., Gleiter, H., Eds.; Wiley-VCH: Weinheim, 2000; p 154. (b) Warnken, M.; Lazar, K.; Wark, M. *Phys. Chem. Chem. Phys.* **2001**, *3*, 1870.

(17) Klaas, J.; Schulz-Ekloff, G.; Jaeger, N. I. *J. Phys. Chem. B* **1997**, *101*, 1305.

10.1021/cm0107732 CCC: $22.00
Published on Web 05/16/2002

stability of, for example, highly dispersed Ti^{IV} oxide species, better than what can be obtained in amorphous SiO_2 or the mesoporous molecular sieve Si−MCM-41. However, the insulating properties of the matrixes prevent the usual recording of changes in the resistivity of such systems as a function of the surrounding gas atmosphere. In a previous paper it has been demonstrated that the sensing behavior, that is, the redox reactions, of these composite materials can be followed by optical detection.[18]

In the present study detailed information about the structure of the titanium oxide species is achieved by EXAFS and XANES measurements and correlated to the redox and sensing properties. Finally, the performance of the best sensing material in detecting deviations of the λ value is tested.

2. Experimental Section

2.1. Materials. Ti^{IV} oxide species stabilized in a NaY−zeolite matrix were prepared by applying methods of chemical vapor deposition (CVD) and ion exchange. NaY zeolite (Si/Al = 2.7) was synthesized following standard recipes.[19]

During chemical vapor deposition (CVD) the NaY zeolite was dehydrated at 673 K for 12 h (heating rate: 2 K/min) and loaded at 373−673 K for 15−30 min in a N_2 stream saturated with $TiCl_4$. Afterward, the bound $TiCl_4$ is hydrolyzed at 373 K in a N_2 stream saturated with water and finally calcined under shallow bed conditions in a stream of dry O_2 at 673 K for 4 h. Details have been described in previous papers.[17,18] For some samples this procedure was repeated two and three times at temperatures of 373 and 673 K.

Ion exchange with $(NH_4)_2TiO(C_2O_4)_2$ in aqueous solution was carried out following a method developed by Liu et al.[20,21] One gram of dried zeolite NaY was suspended in 100 mL of an 5×10^{-3} mol/L aqueous solution of $(NH_4)_2TiO(C_2O_4)_2$ and stirred for 12 h. After the exchanged zeolite was filtrated and washed five times with distilled water, the sample was calcined at 823 K for 12 h (heating rate: 2 K/min). To achieve higher exchange rates for one sample, this procedure was repeated three times.

The Ti content was determined by atomic absorption spectroscopy (AAS) analysis after the Ti zeolites were dissolved in an autoclave with a highly acidic solution ($HF:HNO_3 = 1:4$, 440 K, 12 h).

As reference materials, titanosilicate TS−1, prepared according to the wetness impregnation method[22,23] and possessing almost exclusively tetrahedrally coordinated Ti atoms on framework positions, and commercially available TiO_2 (HOM UV100, Sachtleben Co., anatase, particle diameter: 4−10 nm) were used.

The designations of the samples and the corresponding Ti contents are listed in Table 1.

2.2. Methods. To control the crystallinity of the Ti zeolites, (i) X-ray diffractograms (XRD) were recorded in a Seiffert diffractometer with Bragg−Brentano geometry using Cu Kα radiation under ambient conditions and (ii) adsorption measurements were carried out with a Grimm BET Automatic Surface Analyzer by physisorption of N_2 at 77 K. The adsorbed amounts of nitrogen represent the available pore volumes in the samples, giving an indication of the regular porosity of the zeolite material and a possible pore blockage by the guest compounds. Although BET surface areas are doubtful for type I isotherms, we also calculated the "BET surface areas" because these values are often found in the literature.

Table 1. Ti^{IV} Oxide Species in NaY: Sample Code, Temperature, and Number of Cycles for Loading with $TiCl_4$, Ti Content (wt %), Pore Volume (cm^3/g), Determined by Adsorption of N_2, and the Resulting Surface BET Value (m^2/g)

sample	CVD loading temp (K)	no. of cycles	Ti content (wt %)	pore volume (cm^3/g)	BET value (m^2/g)
TiNaY−C1	373	1	1.9	0.267 ± 0.02	750 ± 50
TiNaY−C2	373	3	8.1	0.153 ± 0.02	430 ± 50
TiNaY−C3	673	1	1.3	0.249 ± 0.02	700 ± 50
TiNaY−I1	ion exchange	1	1.1	0.293 ± 0.02	825 ± 50
TiNaY−I2	ion exchange	3	3.4	0.291 ± 0.02	820 ± 50
NaY	parent material			0.295 ± 0.02	830 ± 50

Room-temperature Raman spectra were taken for undiluted samples in a fine capillary of a Jobin Yvon (Division Instr.) spectrometer using a Stabilite 2016 (Spectra Physics) laser at 514 nm for detection.

Diffuse reflectance spectra (UV/vis DRS) under ambient conditions were recorded from 12500 to 50000 cm^{-1} with a Varian Cary 4 spectrometer equipped with a Praying Mantis. Reflectance spectra were converted to Kubelka−Munk values ($F(R_\infty)$)[24] under consideration of a Teflon standard material (LOT 75%, Oriel Co.) and the parent NaY zeolite as reference sample. Samples giving $F(R)$ values higher than 3, exceeding the range where the ($F(R_\infty)$) is linearly proportional to the absorption, were diluted with parent zeolite. The spectra of the diluent and support were subtracted according to the following equation:

$$F(R_\infty^{\text{sample}}) = F\left(\frac{R^{\text{sample+support}}}{0.75R^{\text{LOT75\%}}}\right) - \left(\frac{R^{\text{support}}}{0.75R^{\text{LOT75\%}}}\right)$$

The characterization by photoelectron spectroscopy (XPS) was performed in a Kratos XSAM 800 spectrometer using Mg or Al Kα radiation according to a procedure described elsewhere.[23,25] Elemental ratios have been calculated from the detected signal intensities under consideration of the photoionization cross sections, given by Scofield.[26] Titanium concentrations as low as 1 at. % could be reliably detected.

EXAFS/XANES spectroscopy was carried out at station 8.1 at the SRS Daresbury Laboratories, Cheshire. A Si 111 monochromator was used and calibrated to the Ti K-edge of a Ti metal foil reference (4965 eV). Spectra of the activated samples were collected ex situ in air and at room temperature in transmission or fluorescence mode where appropriate. The samples were pressed into small thin plates. Spectra were calibrated and averaged using EXCALIB and baseline-corrected with EXBACK. XANES spectra were normalized to the edge jump.

The measurement of the sensing properties was carried out by in situ UV/vis DRS in a reaction chamber (Harrick) that is positioned in the Praying Mantis. The powder samples were pressed into 1−1.5-mm-thick wafers and deposited in the reaction chamber. For the in situ experiments the samples were heated to 573−773 K and contacted with mixtures of H_2, CO, or O_2 in Ar. During reduction and oxidation cycles the reflectance was continuously recorded at 16200 cm^{-1}, that is, the wavenumber at which the most pronounced changes occur and which is close to the absorption maximum of the formed Ti^{III} species around 18000 cm^{-1}.[18,27] To obtain similar starting

(18) Grubert, G.; Wark, M.; Jaeger, N. J.; Schulz-Ekloff, G.; Tkachenko, O. P. *J. Phys. Chem. B* **1998**, *102*, 1665.
(19) Kacirek, H.; Lechert, H. *J. Phys. Chem.* **1975**, *79*, 1589.
(20) Liu, X.; Iu, K. K.; Thomas, J. K. *Chem. Phys. Lett.* **1992**, *195*, 163.
(21) Liu, X.; Iu, K. K.; Thomas, J. K. *J. Chem. Soc., Faraday Trans. 1* **1993**, *89*, 1861.
(22) Uguina, M. A.; Serano, D. P.; Ovejero, G.; Van Griecken, R.; Camacho, M. *Appl. Catal. A* **1995**, *124*, 391.
(23) Wark, M.; Koch, M.; Brückner, A.; Grünert, W. *J. Chem. Soc., Faraday Trans.* **1998**, *94*, 2033.
(24) Kortüm, G. *Reflexionsspektroskopie*; Springer: Berlin, 1969.
(25) Tkachenko, O. P.; Shpiro, E. S.; Wark, M.; Schulz-Ekloff, G.; Jaeger; N. I. *J. Chem. Soc., Faraday Trans.* **1993**, *89*, 3987.
(26) Scofield, J. H. *J. Electron. Spectrosc.* **1976**, *8*, 129.
(27) Grubert, G. Ph.D. Thesis, University of Bremen, Shaker Verlag, Aachen, 1999.

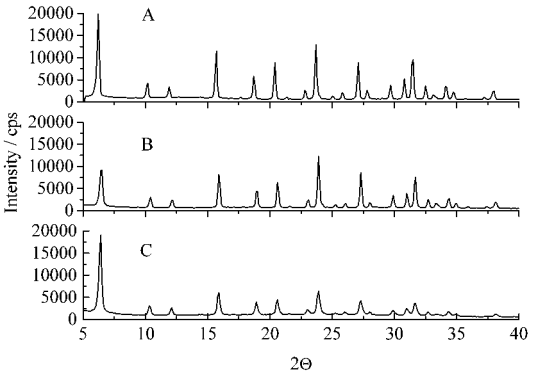

Figure 1. X-ray diffractograms of NaY zeolite parent material (A), Ti−NaY−Cl (B) and TiNaY−I2 (C).

conditions, all samples were pretreated by dehydration in a vacuum at 673 K (heating rate: 2 K/min) for 12 h followed by an oxidation in a stream of 25 vol % O_2 in Ar (80 mL/min) at 823 K for 30 min.

3. Results and Discussion

3.1. Zeolite Crystallinity. The porosity of zeolite samples treated with $TiCl_4$ (TiNaY−C1 and TiNaY−C3, Table 1) has been examined in a previous study.[18] If loaded only once with $TiCl_4$, the samples exhibited a slight (5−10%) decrease of the pore volumes or BET values compared to the parent NaY zeolite (0.295 cm^3/g or 830 cm^2/g), indicating a negligible influence on the porosity of the zeolite. Samples loaded by applying two or three CVD cycles, like sample TiNaY−C2, showed pore volumes or BET values around 0.15 cm^3/g or 450 m^2/g, respectively, pointing to a damage of the zeolite structure and a partial blockage of zeolite cages by titanium oxide species. The partial destruction is also indicated by a reduction of all the XRD reflections by about 30% compared to that in the parent NaY and occurs probably because of an attack by HCl evolved during the repeated CVD loading with $TiCl_4$.

In the X-ray diffractograms of singly loaded samples the relative intensities of the zeolite Y reflections remain constant and their absolute intensities decrease only slightly, indicating a random distribution of the $Ti^{IV}O_x$ (the index *x* signifies that OH groups, or framework oxygen in Si−O−Si bridges of the zeolite, complete the coordination sphere of the titanium) species (Figure 1b).

No reflections of titanium dioxide appear around 2Θ = 25.1 (anatase reflection with highest intensity) in every case, demonstrating the absence of crystalline TiO_2 particles exceeding a diameter of about 3 nm even on the external surface of the zeolite crystallites. This is consistent with the absence of a Raman signal at 144 cm^{-1}, typical for crystalline anatase (particle diameter > 2 nm). Samples with these unwanted anatase fractions that exceed the pore radius of the NaY−zeolite were found occasionally but were not further examined.

Samples prepared by ion exchange showed BET values that are comparable to the value of the parent zeolite (Table 1). The intensity in the X-ray diffractograms is similar to that of the pure NaY (Figure 1a); however, the intensities of reflections at high 2Θ values are slightly reduced in the case of TiNaY−I1. Sample TiNaY−I2, which was two times loaded by ion exchange, exhibits further decrease of the intensities at high 2Θ values (Figure 1c). This indicates that the exchanged

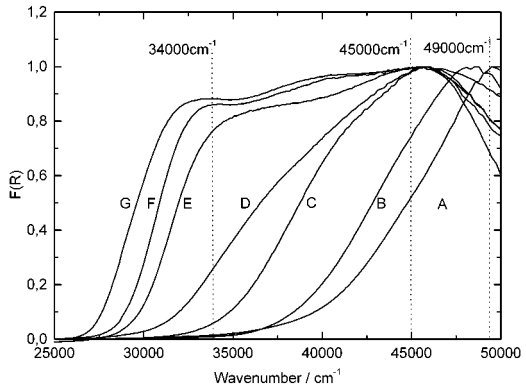

Figure 2. Normalized UV/vis DRS specta recorded at room temperature: TS−1 (A), TiNaY−I1 (B), TiNaY−I2 (C), TiNaY−C3 (D), TiNaY−C1 (E), TiNaY−C2 (F), and bulk anatase (G).

Table 2. Characterization Data for TiNaY and Reference Samples; Point of Intersection of the Tangent through the Point of Inflection of the Absorption Edge and the Abscissa;[18] Binding Energies (BE) and Ti/Si Ratios on the Surface Determined by XPS ($(Ti/Si)_{surface}$) and in the Bulk from AAS ($(Ti/Si)_{bulk}$) of TiNaY and Reference Samples

sample	point of intersection (cm^{-1})	BE Ti $2p_{3/2}$ (eV)	$(Ti/Si)_{surface}$	$(Ti/Si)_{bulk}$
TS−1	42250	459.9 ± 0.2	0.028 ± 0.005	0.032 ± 0.005
bulk anatase	27450	458.5 ± 0.2		
TiNaY−C1	29850	459.1 ± 0.2	0.534 ± 0.005	0.050 ± 0.005
TiNaY−C2	29150	459.2 ± 0.2	0.224 ± 0.005	0.215 ± 0.005
TiNaY−C3	31500	459.2 ± 0.2	0.221 ± 0.005	0.045 ± 0.005
TiNaY−I1	39700	459.3 ± 0.2	0.0199 ± 0.005	0.021 ± 0.005
TiNaY−I2	34200	459.0 ± 0.2	0.0406 ± 0.005	0.064 ± 0.005

titanium species are attached on crystallographically defined positions, that is, TiO^{2+} ions on cation sites of the zeolite.

3.2. Nature of $Ti^{IV}O_x$ Species. Table 2 gives the Ti/Si ratios at the surface ($(Ti/Si)_{surface}$), deduced from the quantification of the intensities of XPS signals of Ti $2p_{3/2}$ electrons in the $Ti^{IV}O_x$ species and Si 2p electrons of the zeolite, in comparison to the average value (Ti/Si_{bulk}) determined by AAS analysis after dissolution of the zeolite crystals in HF:HNO_3. Both samples, which were loaded by ion exchange, show Ti/Si ratios nearly equal to that of TS−1 in which Ti is randomly located on framework positions of the zeolite; that is, no enrichment of titanium species at the outer surfaces of the NaY zeolite crystals is present. This stands in contrast to TiNaY samples loaded once with $TiCl_4$ by CVD for which an enrichment of the titanium species on the outer surface of the zeolite crystals has been found.[18]

Figure 2 represents normalized UV/vis DRS spectra of TiNaY samples and reference materials. All absorption originates from electron charge-transfer transitions from oxygen 2p levels to titanium 3d levels (O → Ti− CT).[28] For all samples the absorption is significantly blue-shifted compared to that of the 4-nm TiO_2 particles and red-shifted compared to the tetrahedrally coordinated Ti in TS−1 with an onset of the absorption around 38000 cm^{-1} and an absorption maximum around 49500 cm^{-1}. In agreement with literature data,[29−32] it can be

(28) Jørgensen, C. K. *Proc. Inorg. Chem.* **1970**, *12*, 101.
(29) Zecchina, A.; Spoto, G.; Bordiga, S.; Ferrero, A.; Leofanti, G.; Petrini, G.; Padovan, M. *Stud. Surf. Sci. Catal.* **1991**, *69*, 251.
(30) Thangaraj, A.; Kumar, R.; Mirajkar, S. P.; Ratnasamy, P. *J. Catal.* **1991**, *130*, 1.

assumed that after the first CVD loading step three different kinds of 5- or 6-fold coordinated $Ti^{IV}O_x$ species are formed.

It is well-known that the π-O → Ti−CT electronic transitions of more or less octahedrally coordinated species exhibit more than one absorption band between 34000 and 50000 cm^{-1}.[17,33] The position of the bands with lowest energy depends strongly on the distortion of the oxygen coordination sphere, that is, the more pronounced the distortion of the octahedral coordination sphere, the higher the energy of the π-O → Ti−CT transition.[28] Thus, the electronic absorption in the region around 34000 cm^{-1} has been assigned to O → Ti−CT in 5- or 6-fold coordinated $Ti^{IV}O_x$ species, which are monofunctionally bound to a single isolated OH group in the zeolite. The absorption around 45000 cm^{-1} originates from electronic transitions in $Ti^{IV}O_x$ species, which are bifunctionally attached to vicinal silanol groups possessing a more distorted coordination sphere.[17] The relative amount of these species is increasing with the temperature of the $TiCl_4$ loading. Absorptions at wavenumbers larger than ≈45000 cm^{-1} cannot be assigned unequivocally because for all 5- or 6-fold coordinated TiO_x species electronic transitions into high-energy levels overlap in that region.

Further CVD cycles lead to a bonding of $TiCl_4$ to the anchored $Ti^{IV}O_x$ species, forming three-dimensional $Ti^{IV}{}_yO_x$ clusters ($y > 1$). These clusters are smaller than 2 nm because the absorption edge resulting from these species remained blue-shifted relative to that of the 4-nm TiO_2 particles; that is, they still show the effect of size quantization.[34]

The UV/vis DRS spectra of the ion-exchanged TiNaY samples showed no difference before and after calcination and the electronic transitions indicate the presence of isolated titanium oxide species. The UV/vis spectrum of the singly exchanged TiNaY−I1 sample is comparable to that of TS−1 with a slightly red-shifted absorption maximum at 48000 cm^{-1} (Figure 2). That leads to the conclusion that the oxygen coordination sphere around the Ti is drastically deviating from the octahedral symmetry; probably TiO^{2+} ions are present on cationic sites of the zeolite. Sample TiNaY−I2 exhibits a spectrum more comparable to that of sample TiNaY−C3, indicating a slightly less distorted coordination sphere for at least some of its Ti oxide species.

For all the TiNaY samples binding energies for the Ti $2p_{3/2}$ electrons around 459.2 eV were measured, which is between the values found for tetrahedrally coordinated framework Ti in TS−1 and for octahedrally coordinated Ti in crystalline anatase (Table 2).

To obtain more detailed information on the coordination sphere of the different $Ti^{IV}O_x$ species, XANES and EXAFS spectra have been recorded. The pre-edge peaks in Ti K-edge XANES measurements are sensitive to the environment of the titanium atoms.[35,36] Octahedrally coordinated titanium species, for example, in anatase, exhibit multiple pre-edge peaks of low intensity between 4960 and 4979 eV. Deviations from the octahedral symmetry lead, in general, to (i) an increase of the intensity of the center peak, (ii) a shift of the pre-edge peak toward lower energies, (iii) a decrease of the intensity of the satellite peaks, and (iv) a smaller full-width at half-maximum (fwhm). Tetrahedrally coordinated titanium atoms such as those in TS−1 show only one high intensive pre-edge peak.[37] The normalized Ti K-edge XANES spectra are represented in Figure 3. The corresponding parameters (position, normalized height, and fwhm) are listed in Table 3. Lorentzian and Gaussian functions were used for fitting of the pre-edge peaks to determine the peak positions, intensities, and fwhm. The reference materials TS−1 and anatase show typical XANES spectra and parameters for a tetrahedral and octahedral environment of the titanium atoms, respectively.[32,37] For TS−1 the height of the pre-edge peak (normalized to the edge) in the XANES spectrum is only 0.3, which is lower than values reported earlier, being around 0.5.[32,35] This might result from slight distortions at some of the Ti centers in the zeolite framework occurring because of the adsorption of some water molecules. A decrease of the normalized peak height with increasing water content in TS−1 samples has been recently reported.[32] However, it is important to mention that the adsorbed amounts of water must be very low because a silicalite, in general, is very hydrophobic and because no differences in the UV/vis DRS spectra prior to and after evacuation of the sample were observed.

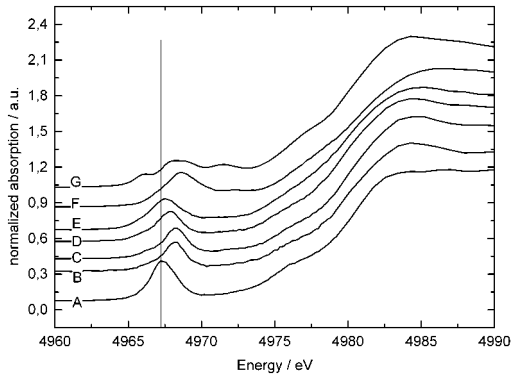

Figure 3. Normalized Ti K-edge XANES spectra recorded at room temperature: TS−1 (A), TiNaY−I1 (B), TiNaY−I2 (C), TiNaY−C3 (D), TiNaY−C1 (E), TiNaY−C2 (F), and bulk anatase (G).

Table 3. Ti K-Edge XANES Parameter of the Pre-edge Peaks for TiNaY and Reference Samples; Height of the Pre-edge Peaks Was Normalized to the Edges

sample	position eV)	normalized height	fwhm (eV)
TS−1	4967.4	0.3	2.0
bulk anatase	4968.6	0.17	2.9
TiNaY−C1	4967.5	0.20	2.5
TiNaY−C2	4967.9	0.20	2.8
TiNaY−C3	4967.8	0.20	2.2
TiNaY−I1	4968.2	0.21	1.7
TiNaY−I2	4968.2	0.21	1.8

(31) Trong On, D.; Le Noc, L.; Bonneviot, L. *J. Chem. Soc., Chem. Commun.* **1996**, 299.
(32) Ikeue, K.; Yamashita, H.; Anpo, M.; Takewaki, T. *J. Phys. Chem. B* **2001**, *105*, 8350.
(33) Lever, A. B. P. *Inorganic Electronic Spectroscopy*; Elsevier: Amsterdam, 1984.
(34) Aronson, B.; Blanford, A. E.; Stein, A. *Chem. Mater.* **1997**, *9*, 2842.
(35) Zhang, W.; Fröba, M.; Wang, J.; Tanev, P. T.; Wong, J.; Pinnavaia, T. *J. Am. Chem. Soc.* **1996**, *118*, 9164.
(36) Behrens, P.; Felsche, J.; Vetter, S.; Schulz-Ekloff, G.; Jaeger, N. I.; Niemann, W. *J. Chem. Soc., Chem. Commun.* **1991**, 678.
(37) Anpo, M.; Yamashita, H.; Ichihashi, Y.; Fujii, N.; Honda, M. *J. Phys. Chem.* **1997**, *101*, 2632.

The TiNaY samples prepared by the CVD method (C1−C3) exhibit peak positions, peak heights, and fwhm that are between the values of TS−1 and anatase. This indicates again a distortion from the octahedral environment of the titanium atom. $Ti_y^{IV}O_x$ clusters, which are mainly present in sample TiNaY−C2, exhibit parameters of the center pre-edge peak (position at relative high energy and high fwhm) that are most comparable to those of anatase. This might point to less distorted octahedrally coordinated titanium atoms. However, the satellite peaks of sample TiNaY−C2 have very low intensities.

The ion-exchanged samples, with the assumed TiO^{2+} ions on cation sites of the zeolite, exhibit unusual pre-edge parameters. Although the peak positions and heights are at energies and intensities like those for TiNaY−C2 and −C3, the fwhm is even lower than the value calculated for TS−1 (Table 3). Multiple ion exchange leads to a slight broadening of the pre-edge peak, which indicates a fraction of monomolecularly bound $Ti^{IV}O_x$ species. Similar pre-edge parameters were found for a number of different compounds with 5-fold coordinated Ti.[38] Compounds with 5-fold coordinated Ti exhibit relatively high intensity of the pre-edge peak in comparison to more octahedrally coordinated species (≈60% of the intensity of tetrahedral Ti), which results from p−d orbital mixing in the $(TiO)O_4$ site, making the 1s−3d transition allowed and thus giving a higher intensity than that found in octahedral symmetry. Although the energy of the transition in ion-exchanged samples is more similar to that in the octahedral form, the other two parameters indicate a nonoctahedral environment. The significantly different chemical environment of Ti on cationic sites near the negatively charged tetrahedral Al centers in the zeolite framework is likely to result in a change in energy of the 1s−3d transition.

Further information about the local structure of the titanium atoms in the $Ti^{IV}_yO_x$ cluster species is achieved from EXAFS data. Figure 4a−c shows the experimental and calculated reciprocal space and real space (Fourier transform) spectra for TiNaY−C1, −C3, and −I1. The parameters used for the first shell calculations are listed in Table 4. The values found for the reference materials, TS−1, and anatase are in good agreement with the data found in the literature.[39] In comparison to anatase, where nondistorted octahedrally coordinated Ti is present, all the Ti−O distances and coordination numbers *N*, found for the Ti^{IV} oxide/zeolite composites, are significantly decreased. The decreased coordination numbers and Ti−O distances observed for samples TiNaY−C3 and TiNaY−C2 in comparison to those for sample TiNaY−C1 lead to two conclusions, which result in the proposed structures depicted in Chart 1. First, bifunctionally bound mononuclear $Ti^{IV}O_x$ species, which are mainly present in sample TiNaY−C3, reveal presumably 5-fold oxygen coordination as indicated by a lower coordination number and a shorter Ti−O distance in comparison to those of samples with monofunctionally bound $Ti^{IV}O_x$ species, almost exclusively present in TiNaY−C1, exhibiting more octahedral-like coordination (Chart 1A,B). Second, although for the 3-fold loaded sample TiNaY−C2, containing $Ti^{IV}_yO_x$ cluster, a relatively large uncertainty in the coordination numbers occurs, it can be stated that the calculated average coordination number *N* is slightly reduced in comparison to TiNaY−C1 and anatase. This can be related to a high number of Ti atoms at the surface of the assumed $Ti^{IV}_yO_x$ cluster, which are close to the pore walls of the growth, restricting zeolite cages. Oxygen atoms of the zeolite framework form dative bonds to the Ti (Chart 1C). The dative binding is favored because with it a cleavage of Si−O−Si or Si−O−Al bonds in the zeolite is avoided. The XANES interpretation of the presence of $Ti^{IV}_yO_x$ clusters in this sample is supported by the observation of a short Ti−Ti distance at 3.06 Å (coordination number of 1.2, $\sigma = 0.0025$ Å^2).

For the ion-exchanged samples the short average Ti−O distance of the samples of about 1.77 Å rules out the possibility of octahedral coordination. However, it indicates the formation of a Ti═O bond. Thus, the first Ti−O shell was fitted with two oxygen shells (Figure 4, Table 4). Indeed, an additional shell at a distance of ≈1.6 Å was found, which is similar to Ti═O distances reported.[38] Presumably, the ammonium titanyl oxalate precursor exchanges with cationic sites of the zeolite and after decomposition the titanyl bond is retained.

It was suggested that ammonium titanyl oxalate forms TiO^{2+} or dimeric $Ti_2O_3^{2+}$ in the aqueous phase under ion-exchange conditions.[21] If a Ti atom is used as the second neighbor in the EXAFS fitting procedure of TiNaY−I1, a Ti−Ti distance at 3.01 Å is found. This would be a reasonable distance for a dimeric Ti species with bridging oxygen ions. However, the freely fitted coordination number of 0.5 ($\sigma = 0.004$ Å^2) is rather low, indicating a minor contribution of $Ti_2O_3^{2+}$ ions. With Si as the second neighbor with a coordination number of 1.9 ($\sigma = 0.001$ Å^2) a distance of 3.24 Å is found, which is similar to Ti−Si distances reported earlier.[38] In agreement with the findings described in ref 40, the quality of the fit in relation to the experimental data is significantly improved with the silicon shell ($R = 30.9$ for Si, $R = 32.6$ for Ti). Although an unambiguous answer cannot be contemplated because the difference in the backscattering amplitude between Ti and Si or Al is rather small, it is thus assumed that the majority of Ti species in TiNaY−I1 is indeed rather isolated and the TiO^{2+} cations are interacting with the zeolite framework.

3.3. Redox Properties. After the samples were reduced with 25 vol % H_2 in Ar for 2 h at 673 K, a new absorption band ranging from 18200 to 16100 cm^{-1} appeared in the UV−vis DRS spectra of TiNaY−C1 and TiNaY−C3 and to a small extent also in TiNaY−I2. For TiNaY−C2 and bulk anatase samples a continuous increase of the $F(R)$ values at wavenumbers lower than 18000 cm^{-1} has been found.[18] The TS−1 and TiNaY−I1 sample, however, show no significant differences in the Kubelka−Munk spectra between the reduced and the oxidized material, demonstrating that the tetrahedrally coordinated titanium species in TS−1 and titanyl species at cation sites are not reducible. In sample TiNaY−I2 the manifold titanyl ion exchange leads additionally to a small fraction of reducible $Ti^{IV}O_x$

(38) Farges, F. *J. Non-Cryst. Solids* **1996**, *204*, 53.
(39) Trong On, D.; Bonneviot, L.; Bittar, A.; Sayari, A.; Kaliaguine, S. *J. Mol. Catal.* **1992**, *74*, 233.
(40) Stockenhuber, M.; Hudson, M. J.; Joyner, R. W. *J. Phys. Chem. B* **2000**, *103*, 3370.

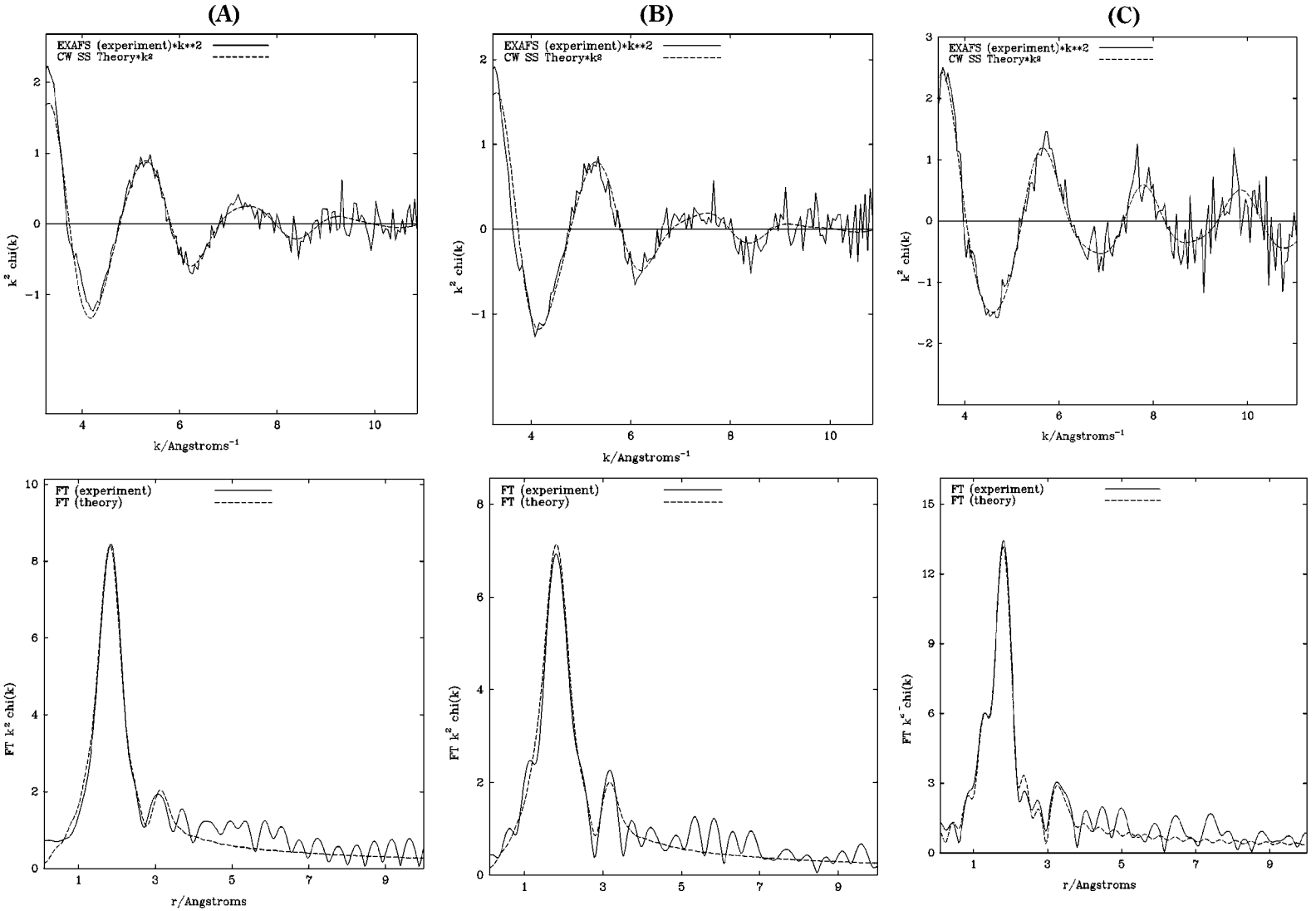

Figure 4. EXAFS oscillations and FT magnitude of samples TiNaY−C1 (A), TiNaY−C2 (B), and TiNaY−I1 (C).

Table 4. EXAFS Results for the First-Coordination Sphere (Ti−O)[a]

sample	*N*	*D* (Å)	σ (Å^2)
TS−1	4.4 ± 0.66	1.813 ± 0.011	0.009 ± 0.003
bulk anatase	5.7 ± 0.42	1.922 ± 0.010	0.033 ± 0.002
TiNaY−C1	5.4 ± 0.30	1.878 ± 0.013	0.036 ± 0.004
TiNaY−C2	4.8 ± 1.0	1.855 ± 0.02	0.033 ± 0.007
TiNaY−C3	4.2 ± 1.1	1.800 ± 0.023	0.023 ± 0.008
TiNaY−I1	4.4 ± 0.8	1.78 ± 0.014	0.003 ± 0.001
	1.1 ± 0.7	1.58 ± 0.023	0.001 ± 0.005
TiNaY−I2	4.7 ± 0.9	1.778 ± 0.017	0.023 ± 0.005
	1.2 ± 0.8	1.61 ± 0.07	0.041 ± 0.02

[a] *N* = coordination number; *D* = interatomic distance (Ti−O); σ = Debye−Waller factor.

Chart 1. Illustration of Possible Structures of Mononuclear $Ti^{IV}O_x$ Species Monofunctionally Bound with 6-fold Oxygen Coordination (A) and Bifunctionally Bound with 5-fold Coordination (B) and of $Ti^{IV}_yO_x$ Cluster ($y > 1$) in the Pores of the NaY Zeolites (C)[a]

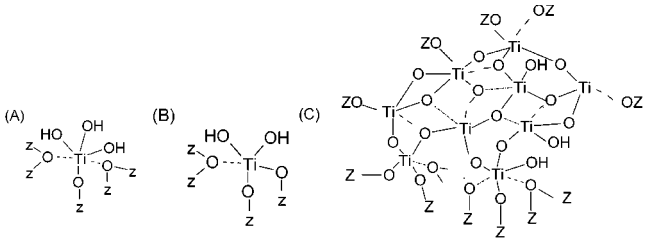

[a] The dashed lines assign a coordinative bond to the Ti atom. Z stands for a Si or Al of the zeolite framework.

species as found in the TiNaY−CVD samples. This observation is in good agreement with the XANES and UV/vis DRS results.

For all reducible TiNaY samples the changes in $F(R)$ values occurring during reduction are completely reversible in contact with oxygen. The reoxidation, that is, the healing of the oxygen vacancies in the titanium oxide species, which have been formed during reduction, is completed for all samples within about 15 s and, thus, faster than the reduction. Because of the bigger cross section of oxygen in comparison to hydrogen, the presence of barriers for the gas diffusion in the zeolite pore system can be ruled out.

The evolution of the $F(R)$ values at a fixed wavenumber (16200 cm^{-1}) with time represents the degree of reduction of Ti^{IV} to Ti^{III} species achieved within that period. Figure 5 shows exemplarily the reduction of sample TiNaY−C1 at different temperatures.

On the basis of pseudo-first-order kinetics and the presence of three different $Ti^{IV}O_x$ species,[18] for each temperature three reduction constants, that is, one for each $Ti^{IV}O_x$ species, were found. The $Ti^{IV}O_x$ species bifunctionally bound to the zeolite reveal the highest reduction rate constant (k_1) followed by that of the $Ti^{IV}O_x$ species on the external surface of the zeolite crystallites (k_2). The lowest reducibility was found for $Ti^{IV}O_x$ species, which are monofunctionally bound to the zeolite (k_3). The reduction constants are listed in Table 5.

The temperature dependence of the reduction constants result in straight lines in the Arrhenius plot (Figure 6). The activation energies for the three different $Ti^{IV}O_x$ species and the pre-exponential factors are given in Table 5. The concentrations of the different reducible TiO_x species from the evaluation of the kinetic data are

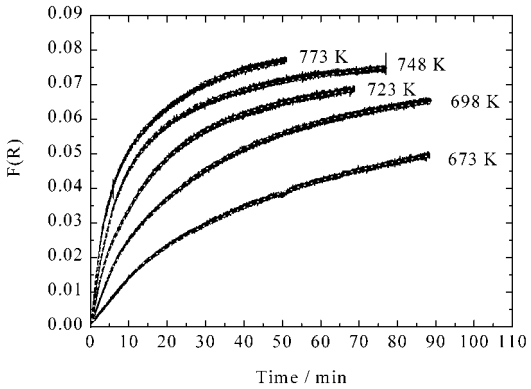

Figure 5. Reduction of TiNaY−C1 at different temperatures. The dotted lines are nonlinear curve fits assuming three independent pseudo-first-order kinetics. Fit function: $[Ti(III)] = [Ti(IV)_{1s}]_0 + [Ti(IV)_{1p}]_0 + [Ti(IV)_{2p}]_0 - [Ti(IV)_{1s}]_0 \exp(-k_1 t) - [Ti(IV)_{1p}]_0 \exp(-k_2 t) - [Ti(IV)_{2p}]_0 \exp(-k_3 t)$.

Table 5. Reduction Rate Constants (k_i), Activation Energies (ΔE_a), and Pre-exponential Factors (A) for Mononuclear TiO_x Species[a]

k_i (s^{-1})	773 K	748 K	723 K	698 K	673 K	ΔE_a (kJ/mol)	A (s^{-1})
k_1	1.6	1	0.77	0.43	0.24	80	4.5×10^5
k_2	0.13	0.11	0.07	0.04	0.018	87	1.2×10^5
k_3	0.03	0.017	0.01	0.005	0.002	100	1.8×10^5

[a] The errors in ΔE_a and A are about ±10%.

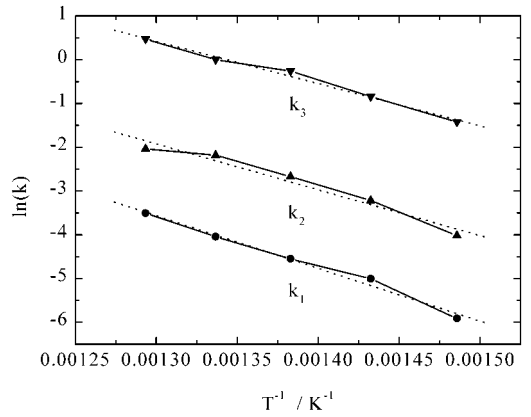

Figure 6. Arrhenius plot of the temperature dependence of the reduction rate constants.

Table 6. Concentrations of TiO_x Species Located at the Surface ($Ti(IV)_s$), Monofunctionally Bound in the Pores ($(Ti(IV)_{1p})$ or Bifunctionally Bound in the Pores ($Ti(IV)_{2p}$) of NaY Zeolite

sample	$[Ti(IV)_s]_0$ (at. %)	$[Ti(IV)_{1p}]_0$ (at. %)	$[Ti(IV)_{2p}]_0$ (at. %)
TiNaY−C1	63	33	5
TiNaY−C3	41	15	44
TiNaY−I2	56	9	35

listed in Table 6. The reducible TiO_x species in sample TiNaY−I2 prepared by multiple ion exchange are mainly located at the outer surface of the zeolite (56 at. % of the reducible $Ti^{IV}O_x$ species). The reducible $Ti^{IV}O_x$ species in the pores of the NaY zeolite are mainly bifunctionally bound (35 at. %).

The activation of hydrogen has been assumed as the rate-limiting step. This is supported by the determined activation energies, which are on the same order of magnitude than energies found for the dissociative adsorption of hydrogen on TiO_2 with a defect structure (≈80 kJ/mol).[41,42] For bifunctionally bound $Ti^{IV}O_x$ spe-

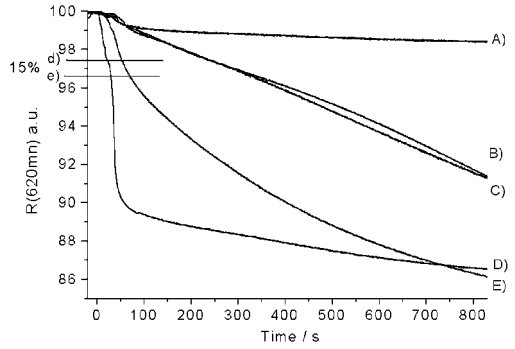

Figure 7. Response times and sensitivities toward reduction with H_2. Samples: TiNaY−I2 (A), TiNaY−C2 (B), bulk anatase (C), TiNaY−C3 (D), and TiNaY−C1 (E). The lines (d) and (e) denote 15% of the total decrease of the reflection for sample TiNaY−C3 and TiNaY−C1, respectively.

cies both the pre-exponent factor and the activation energy are responsible for the high k_1 value. This leads to the conclusion that the structure of the distorted bifunctionally bound species, possessing most likely 5-fold oxygen coordination, makes an activation of hydrogen more feasible than the more octahedral-like monofunctionally bound species. The entropy of the activated state mainly determines the value of the pre-exponential factor: the higher the loss of entropy during the H_2 adsorption, the lower the pre-exponential factor. Lower oxygen coordination numbers, as in the bifunctionally bound $Ti^{IV}O_x$ species, enable more possibilities for the attack of the hydrogen and, thus, reduce the entropy. For tetrahedral Ti species in the zeolite framework and $Ti{=}O^{2+}$ on cation sites, it can be assumed that a high activation energy for the adsorption of hydrogen is very likely responsible for their nonreducibility.

For a detailed evaluation of the reduction parameters for the $Ti^{IV}{}_yO_x$ clusters in the multiple loaded TiNaY−C2 sample, these easy pseudo-first-order kinetics are no longer valid. For the description of their reduction, an autocatalytic mechanism has been attempted.[27]

3.4. Sensing Properties. To determine the sensing properties of these materials, that is, sensitivity and response time, the used time-dependent reflectance raw data were not converted to Kubelka−Munk values. The decreasing reflectance during reduction corresponds to an increasing absorption that is proportional to the concentration of formed Ti^{III} species in the samples. The response time (Δt_R) is defined as the time necessary to achieve a decrease in reflectance of 15% of its final value obtained after complete reduction. The sensitivity (ΔR_S) is the difference in reflectance before reduction and at $t = \Delta t_R$.

Figure 7 shows the response curves used for the determination of Δt_R and ΔR_S for a reduction with 25 vol % H_2 at 773 K. The response times and sensitivities for the reduction depend strongly on the present Ti^{IV} oxide species; the obtained values are listed in Table 7. As expected from the redox data, sample TiNaY−C3, possessing the highest amount of $Ti^{IV}O_x$ species that are bifunctionally bound to the zeolite and reveal the highest reduction rate constant (k_1), shows the shortest response time. Moreover, the ion-exchanged sample

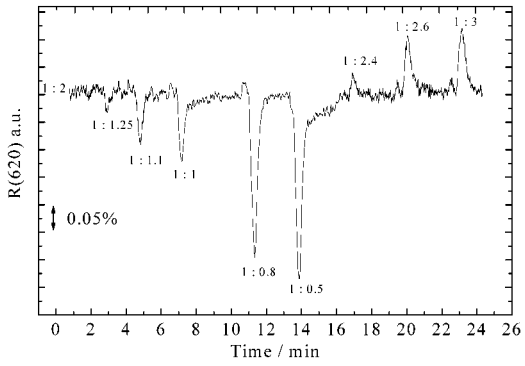

Figure 8. Monitoring of pulsed deviations from a soichiometric mixture (O_2:CO = 1:2); sample: TiNaY−C3. The values at the peaks are the corresponding O_2:CO ratios used for the 5-s pulse for simulating λ deviations.

Table 7. Response Time (Δt_R) and Sensitivity (ΔR_S) of Samples Containing Different Ti Oxide Species

sample	Δt_R (s)	ΔR_S (%)	sample	Δt_R (s)	ΔR_S (%)
TiNaY−C1	50	3.25	TiNaY−I2	19	0.33
TiNaY−C2	226	2.5	bulk anatase	700	7.5
TiNaY−C3	18	2.5			

TiNaY−I2, containing also highly distorted $Ti^{IV}O_x$ species, exhibits also a very short response time; however, the sensitivity is low because of its low content of reducible $Ti^{IV}O_x$ species. Samples containing bulk TiO_2 or $Ti^{IV}{}_yO_x$ clusters show long response times. The high sensitivity of the bulk anatase sample results from its much higher content of Ti atoms.

Relevant temperatures for sensing of exhaust gases are around 1073 K. However, experiments under these temperatures cannot be carried out with the present diffuse reflectance chamber for in situ measurements. Therefore, for the samples with mononuclear species, that is, TiNaY−C1 and −C3, an extrapolation of the response time and sensitivity to higher temperatures has been applied. For this the reaction constants for 1073 K for the different Ti^{IV} oxide species were calculated from the Arrhenius equation. In the next step the reduction curve $F(R_\infty)$ versus time at 1073 K was calculated from the reduction constants and the estimated concentrations of the different Ti^{IV} oxide species. Afterward, the time-dependent $F(R_\infty)$ curve was converted to reflectance spectra by applying the reverse Kubelka−Munk function ($R_\infty = F(R_\infty) - \sqrt{(1+F(R_\infty))^2-1} + 1$). The resulting response times, 0.3 and 0.7 s for sample TiNaY−C3 and −C1, respectively, are comparable to those found for solid-state electrolyte sensors at this temperature.[43]

The detection of alterations in mixtures of hydrocarbons and O_2 is important in lean burning in the motors of vehicles (λ value). In this process CO is a intermediate, and thus the optical registration of deviations of CO:O_2:Ar mixtures (starting composition: CO:O_2:Ar = 1:2:1 (Ar as diluent), flow rate = 80 mL/min) on hosted Ti^{IV} oxide clusters was tested at 773 K. For pulsing the composition of the mixtures the concentrations of either CO or O_2 were varied for periods of 5 s from the λ ratio of O_2:CO = 1:2. The tests have been carried out with sample Ti−NaY−C3, which contains the highest fraction of the best reducible distorted $Ti^{IV}O_x$ species. From Figure 8 it can be seen that it is possible to monitor

(41) Göpel, W.; Rocker, G.; Feierabend, R. *Phys. Rev. B* **1983**, *28*, 3427.
(42) Raupp, G. B.; Dumesic, J. A. *J. Phys. Chem.* **1985**, *89*, 5240.

deviations of the λ ratio by measuring the changes in reflectance. The response time amounts only to a few seconds, and the changes of the reflectance are approximately proportional to the alterations in the concentrations. However, the sensitivity is low because of a relatively large dead volume in the test apparatus, leading to a broadening of the gas inlet pulse. For further studies the experimental setup has to be improved in this respect.

4. Conclusions

Highly dispersed mononuclear and clustered Ti^{IV} oxide species have been stabilized in the pores of Y-type zeolites. The structure and reduction behavior of the embedded Ti^{IV} oxide clusters can be tailored dependent on the methods applied for their encapsulation, either chemical vapor deposition or ion exchange. XANES/EXAFS spectra in combination with XPS and DR−UV/vis studies reveal the presence of mononuclear $Ti^{IV}O_x$ species with a low distorted octahedral oxygen coordination sphere after single chemical vapor deposition at 373 K, whereas a higher temperature (773 K) leads to a preferred formation of mononuclear species with a highly distorted 5-fold coordination. The latter species show the highest reaction rates toward reduction with H_2 or CO. Multiple CVD treatments result in the formation of three-dimensional $Ti^{IV}_yO_x$ ($y > 1$) clusters, mostly located in the zeolite pore system, with a less distorted penta- or octahedral oxygen coordination sphere around the Ti centers. The higher nuclearity of the clusters reduces the reduction rate.

When the ion-exchange method is applied, TiO^{2+} and to a small extent $Ti_2O_3^{2+}$ ions with a retained Ti═O double bond are formed on cationic sites of the zeolite; these species can hardly be reduced.

The following observed properties of zeolite-supported Ti oxide species, formed by chemical vapor deposition, toward H_2, CO, and O_2 atmospheres at 773 K render these composites an interesting material for alternative sensing using optical detection: (i) their stability as demonstrated by a complete reversibility of the extinction for a large number of redox cycles, (ii) their high sensitivities, (iii) their short response times, which can be extrapolated to be <1 s at 1073 K, and (iv) the prospect of a more feasible miniaturization compared to that of ZrO_2-based oxygen sensors.

Acknowledgment. We thank Prof. Dr. G. Schulz-Ekloff and Prof. Dr. N. I. Jaeger (University of Bremen, Germany) and Prof. Dr. R. W. Joyner (Nottingham Trent University, U.K.) for fruitful discussions. The SRS at Daresbury Laboratories, Cheshire, and financial support by the German Science Foundation (SCHU 426/9-3) are gratefully acknowledged.

CM0107732

(43) Lagois, J. In *Sensoranwendungen*; Schaumburg, H., Ed.; Teubner B. G. Press: Stuttgart, 1995; p 343.